

High-Gain Circularly Polarized Pentagonal Microstrip Antenna for Massive MIMO Base Station

Raghunath S. Bhadade¹ and Shrinivas P. Mahajan²
 Department of Electronics & Telecommunication
 College of Engineering, Pune, Maharashtra, India
¹raghunath.bhadade@mitpune.edu.in
²spm.extc@coep.ac.in

Abstract — In this paper we propose a high-gain circularly polarized (CP) pentagonal microstrip antenna on a suspended substrate for Massive MIMO BS applications. The Massive MIMO is one of the key component to be incorporated in the 5G applications. The proposed antenna is successfully simulated using HFSS 13.0v, fabricated on a FR-4 substrate and measured. The proposed antenna exhibits a much higher gain of 6.17 dB, improved impedance bandwidth of 171.9 MHz ($S_{11} = -10$ dB), and axial ratio bandwidth (< 3 dB) of 135 MHz at 2.45 GHz (ISM band). The inter-element spacing of linear and planar antenna array for the Massive MIMO BS is confirmed using systemVue. Also, 2×2 MIMO antenna is simulated using HFSS. The measured and simulated results of the antenna are found in good agreement.

Keywords; *Microstrip Antenna, Massive MIMO, Input impedance, Return loss.*

A. INTRODUCTION

In wireless applications such as LTE, WLAN, and WiMAX, microstrip antennas play a crucial role. The major drawback of these antennas are inadequate gain and impedance bandwidth (BW).

The need of modern communication systems is to provide higher data rates for the required applications. MIMO does this without heightening the transmitter power or bandwidth. Hence, MIMO is popular in wireless communication for more than ten years. MIMO exploits multipath components (MPCs) rather than mitigating it to provide higher data throughput. Thus, antenna technologies are the key to increase the network capacity [3], [4] and [9].

Nowadays, MIMO – OFDMA (Orthogonal Frequency Division Multiple Access) plays a vital role in 4G and beyond wireless communications to enhance the data rates over uplink and downlink channels at a reasonable cost. The LTE and its variants were evolved from GSM and UMTS. The WiMAX and its variants were evolved from IEEE 802.16e amendments. These two are the major candidates for 4G technology [15].

Reduced radiated power, excellent throughput and service everywhere in the cell with greater simplicity in signal processing are the main benefits of the Massive MIMO [5] and [13]. Massive MIMO is also known as —Large-Scale

Antenna Systems” or —Very Large MIMO” or —Hyper MIMO” or —Full-Dimension MIMO” or —ARGOS”. It serves tens of terminals in the same time-frequency resource using antenna array with few hundred radiating elements in the structure. Aggressive spatial multiplexing is used in Massive MIMO for increasing the capacity. Thus, more antennas, more capacity, and enhanced reliability [1], [2] and [14].

As Massive MIMO BS uses extra antennas, energy can be focused into smaller regions of space. This leads to enormous improvements in radiated energy efficiency and throughput. Massive MIMO is a scalable to any desired degree on the number of radiating elements [7], [8], and [13]. The major challenges for designing Massive MIMO BS antenna are compact and low profile, high gain to reduce cost of RF chains, low mutual coupling (or high isolation), centralized and distributed, multi-Freq. bands and mode. Table 1 demonstrates the comparison of existing radiating elements for the Massive MIMO BS antenna.

TABLE 1: EXISTING RADIATING ELEMENT FOR MASSIVE MIMO BS

Ref. Antennas	Radiating element details	Substrate details	Operating Freq. (GHz)	BW (MHz)	Gain (dB/Port)
[4]	Square (Aperture coupled)	Three layered FR4 (ht=1.6mm $\epsilon_r=4.4$)	2.2 to 2.5	230	6.5
[6]	Rectangular (Edge feed, Single polarization, 2×2 antenna array)	Three layered FR4(ht=1.6 mm $\epsilon_r=4.1$)	3.6	230	5.4
[10]	Square (Coaxial probe feed, CP)	Dielectric 880 ($\epsilon_r=2.70$ & $h=3.2$ mm)	3.7	185	--
[11]	Rectangular (Inset feed, Single polarized, and 1×4 antenna array)	TLX-8 ($\epsilon_r=2.55$ & $h=1$ mm)	5.8	200	13
[12]	Square (Corporate feed, Single polarized, and 1×4 antenna array)	--	2.596	194	10

In this paper we present the design, simulation, fabrication and validation of the proposed pentagon microstrip antenna for the Massive MIMO BS operating at 2.45 GHz. The paper is structured as follows: Sec. B details the radiating elements; Sec. C describes the proposed antenna geometry; Sec. D presents the validation of the model and discussions; Sec. E discuss about linear and planar antenna array for the

Massive MIMO BS; this is followed by Conclusions in Sec. F, and Future work in Sec. G respectively.

The contributions of the authors are the design and development of optimal pentagonal microstrip antenna with gain 6.17 dB and impedance bandwidth 171.9 MHz for the Massive MIMO BS.

B. Radiating Elements

The simulation of non-existing microstrip antennas (or elements) such as circular, triangular, and various regular polygons (pentagon to octagon) for Massive MIMO BS are presented in this section. The assortment of radiating element for the Massive MIMO BS based on the challenges stated in introduction plays a vital role. The gain, impedance bandwidth, and physical area of these elements were compared.

The designing of the radiating elements starts from the selection of the center frequency of the operating band. The 2.45 GHz is the center frequency of a ISM band (2.4 to 2.5 GHz) and is considered for the demonstration purpose. Out of numerous feeding techniques, the radiating element is excited with the help of a coaxial probe-feed. The inner and outer conductor of a coaxial probe is soldered to main radiating patch and ground plane respectively. The impedance of a radiating element and source of excitation is based on the location of the feed point. This feeding technique is common, the most popular and has low spurious radiation. For the higher data rate applications (4G and beyond), the thicker substrate (in this study) is used and therefore it needs a longer pin SMA connector. The radiating elements were simulated using commercially available SMA connector with probe dimensions (inner conductor of 0.65mm, dielectric of 0.85mm and the outer conductor of 1.5 mm). The FR-4 substrate (cheaper and easily available than others) is used for simulations, analysis, and validation. All radiating elements were simulated using HFSS 13.0v (Finite Element Method) solver for electromagnetic (EM) structure.

B.1. CIRCULAR AND TRIANGULAR MICROSTRIP ELEMENT

The dimensions of the circular and triangular microstrip element can be calculated by using the equation (1) and (2) respectively.

$$a = \frac{1.8412 c}{2\pi f_r \sqrt{\epsilon_r}} \quad (1)$$

$$s = \frac{2 c}{n f_r \sqrt{\epsilon_r}} \quad (2)$$

Where 'a' is the radius of circular microstrip antenna, c is the velocity of EM waves in free space, fr and ϵ_r are the

resonant frequency and relative dielectric constant of the substrate respectively, and 's' is the side length of the triangular (n = 3) microstrip antenna. The area of circular microstrip antenna is computed by using the standard expression πr^2 . The area of triangular microstrip antenna can be estimated by using equation (3). Table 2 gives the consequences for the circular and triangular microstrip element.

TABLE 2: SIMULATED RESULTS FOR CIRCULAR AND TRIANGULAR MICROSTRIP ELEMENTS AT 2.45 GHZ

Radiating elements	Theoretical		Simulated		BW (MHz)	Gain (dB)
	Dimensions (mm)	A* (mm ²)	Dimensions (mm)	A* (mm ²)		
Circular	a = 17.2	929.40	a = 17.2	29.40	50	2.10
Triangular	s = 38.91	55.57	s = 38.45	40.21	40.4	1.61

A* = Area of the radiating element

B.2. REGULAR POLYGON MICROSTRIP ANTENNA

In this section, the simulation and analysis of single coaxial probe feed pentagon to octagon microstrip antennas as another choice of radiating elements for the Massive MIMO BS is deliberated. The regular polygons have identical side lengths. The side length of the various polygons can be estimated by using equation (2). Area of the various regular polygons can be calculated either from its Side length or a Radius (Circumradius) or an Apothem (Inradius). Given the side length, an area of the regular polygon microstrip antenna can be estimated by using equation (3)

$$Area = \frac{s^2 n}{4 \tan\left(\frac{180^\circ}{n}\right)} \quad (3)$$

The results intended for the various regular polygons (n=5 to 8) in terms of gain, impedance bandwidth, and area of radiating elements are given in Table 3.

TABLE 3: SIMULATED RESULTS FOR VARIOUS REGULAR POLYGONS AT 2.45 GHZ

Radiating element	n	Theoretical		Simulated		BW (MHz)	Gain (dB)
		s	A	S	A		
Pentagon	5	23.35	938.06	22.51	871.93	50	2.62
Hexagon	6	19.45	982.85	18.40	879.60	50.5	2.13
Heptagon	7	16.67	1009.82	15.70	896.47	50	2.07
Octagon	8	14.97	1027.81	13.47	876.82	53.3	2.09

n= Number of sides and s = side length (mm)

From Table 2 and 3, it is clear that, the pentagonal microstrip antenna shows improved results in terms of the

gain (2.62 dB) and impedance bandwidth (50 MHz) at 2.45 GHz with smaller physical patch area (871.93 mm²). Therefore, the pentagonal microstrip antenna is chosen as a radiating element for the Massive MIMO BS.

C.Proposed Radiating Element

In this section, we present the modified pentagonal microsteip antenna. The modification to this antenna is in terms of circularly polarization, reduced physical area, and enhanced gain, improved impedance bandwidth.

C.1. CIRCULAR POLARIZATION (CP)

Microstrip antenna normally supports Linear polarization (LP); however, by doing certain modifications to the basic antenna geometry and /or feed, CP can also be achieved [19]. Orthogonal polarization (or dual feed) is basic idea behind CP radiation. LP and CP radiations can be received by a single antenna. Also, to improve communications capacity and quality against mutli-path effects, CP antennas are widely used. The role of CP antennas in Massive MIMO BS can serve many tens of terminals in the same time-frequency resource. Axial ratio (AR) is a quality metric for CP antennas. A perfect CP antenna means AR = 1 (or 0 dB). Figure 1 shows, the radiation of Right Hand CP (RHCP) with two orthogonal modes or feed points (feed point 1 and 2). The two feeds encompass identical amplitude but in-phase quadrature.

C.2. SLIT LOADED

In this section, we present the reduction of physical area of the proposed microstrip antenna using loading of the slits on the radiating patch [20]. The radiating element with small aperture is leads to overall weight reduction of the Massive MIMO BS antenna. The RHCP pentagonal microstrip antenna loaded with five slits is shown in Figure 1. The five slits are created by observing the current distribution on the radiating patch using HFSS.

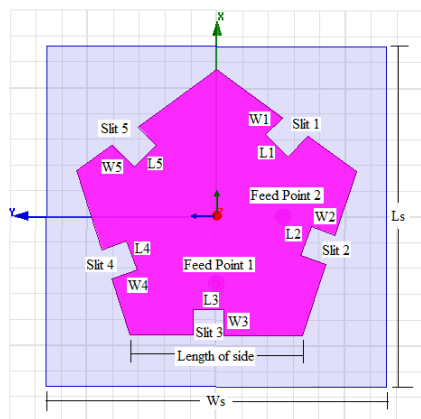


Figure 1. Proposed CP Pentagonal Microstrip Antenna (Feed Point 1 = (- 13, 0) mm, Feed Point 2 = (0, -13) mm)

To obtain the optimum value of gain and impedance bandwidth, slits dimensions (L and W) were varied in a step of 1 mm. The simulated gain and bandwidth for various slit dimenions are compared in Table 4. Based on the experimentation, the optimum slits length (5 mm) and width (4 mm) were used for proposed radiating ellement.

TABLE 4: SLIT DIMENSIONS

Slits dimensions (mm)		BW (MHz)	Gain (dB)
Length (L)	Width (W)		
1	1	6.55	143
2	2	6.57	143
3	3	6.57	140
4	4	6.21	168
5	5	6.16	173

C.3. GAIN AND BANDWISTH ENHANCEMENT

The need of radiating element in Massive MIMO BS is to afford high gain (to reduce the cost of RF chain) and bandwidth (to carry high data rate signals). Several researchers shows that antenna’s gain and bandwidth can be enhanced using impedance matching techniques [14]. To achieve the same objective, the majority of the Massive MIMO testbed employs antenna array with either in-set, edge or corporate feed [6], [11], and [12].

In this section, the suspended substrate technique is used to achive the improvement in gain and bandwidth of the radiating element. The basic antenna geometry of the proposed pentagonal microstrip antenna is shown in Figure 2.

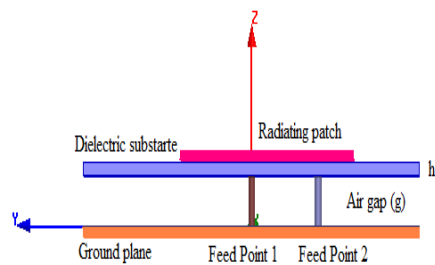


Figure 2. Side view of proposed antenna (Feed Point 1 = (-13, 0) mm, Feed Point 2 = (0, -13) mm)

The presence of an air gap (thicknees g) between the substrate and ground plane reduces the effective dielectric constant. As a result, we observed that, the resonant frequency and bandwidth increases. The antenna canbe tuned from any frequency between 2.4 to 2.5 GHz (ISM

band) by adjusting an air-gap thickness [20]. Also, gain of the antenna can be enhanced by decreasing the ϵ_r [10, 11]. The side length s of the antenna can be estimated by using equation (3) with the substitution of ϵ_r by ϵ_{re} . The term ϵ_{re} is called the effective relative permittivity of the two-layered cavity and is given by equation (4) [20].

$$\epsilon_{re} = \frac{(h+g)\epsilon_r}{(h+g\epsilon_r)} \quad (4)$$

The maximization of the antenna's bandwidth was presented in [17, 18], by using the expression (5)

$$g = 0.16\lambda_0 - h\sqrt{\epsilon_r} \quad (5)$$

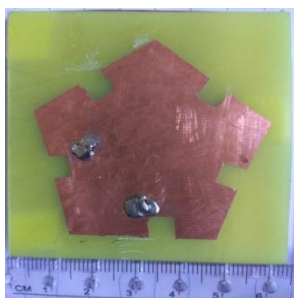
Where λ_0 is wavelength in free space. The optimum value of the air-gap was 6 mm. The CP pentagonal microstrip antenna with 6 mm air-gap shows enhanced gain of 6.17dB and improved impedance bandwidth of 168 MHz without air-gap (Table 3). Table 5 gives the final dimensions of the proposed antenna.

TABLE 5: FINAL DIMENSIONS OF THE PROPOSED ANTENNA

Parameter	Value
Side length (s), mm	33.50
Slits length (L), mm	5.0
Slits width (W), mm	4.0
Dielectric constant (ϵ_r)	4.4
Substrate thickness (h), mm	1.6
Loss tangent	0.0027
Air gap (g), mm	6.0
Ground plane ($L_s \times W_s$), mm	66×66

D. VALIATION OF THE MODEL AND DISCUSSIONS

The RHCP prototype antenna was fabricated as per the design described in previous section with dimensions given in Table 6, is shown in Figure 3. To maintain the uniform current distribution over the ground plane, a foam material (white in colour) is placed below the ground plane. It's effect on slight deviation of the resonant frequency is observed due to change in effective dielectric constant.



(a) Top view



(b) Side view

Figure 3. Fabricated prototype antenna

The experimental set up for the measurement of radiation pattern and gain of the prototype pentagon antenna is as shown in Figure 4. The vector network analyzer (Agilent, 9 KHz to 3GHz) is used as an excitation source ($P_{out} = 0$ dBm at 2.45 GHz) for standard dipole antenna (Transmitting antenna). The received power at 2.45 GHz is measured using the spectrum analyzer (Keysight, 9 KHz to 3 GHz).



(a) Indoor

(b) Outdoor

Figure 4. Experimental set up

The polarization of the receiving antenna is matched to that of the transmitting antenna. The height of transmitting and receiving antenna was kept to $15\lambda_0$ ($\lambda_0 = 120$ mm at 2.45GHz). The receiving antenna was rotated in 10° steps over azimuth span (0° to 360°). The normalized received signal strength (dB μ V) is plotted as a function of theta (degree), as shown in Figure 5.

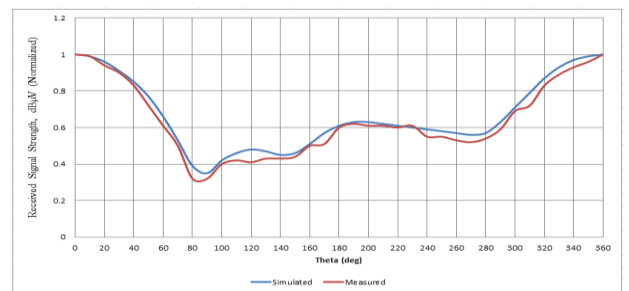


Figure 5. Simulated and measured radiation pattern at 2.45 GHz

We found good agreement in measurement of radiation pattern for indoor and outdoor far-field. The 80° half-power beam-width (HPBW) at far-field is also observed for both the measurements.

Two-antenna method is used to measure the gain of the fabricated antenna using indoor experimental set up. The frequency of the transmitter and receiver was increased in a step of 100 MHz over a frequency span from 2 GHz to 3 GHz. Initially, received signal strength were recorded using

standard dipole antenna at both ends. Later on readings were taken using actual fabricated antenna at receiving end with dipole antenna at transmitting. The gain of actual antenna was calculated using comaprision. The actual antenna shows gain of 6.01 dB with respect to dipole antenna at 2.45 GHz, is as shown in Figure 6.

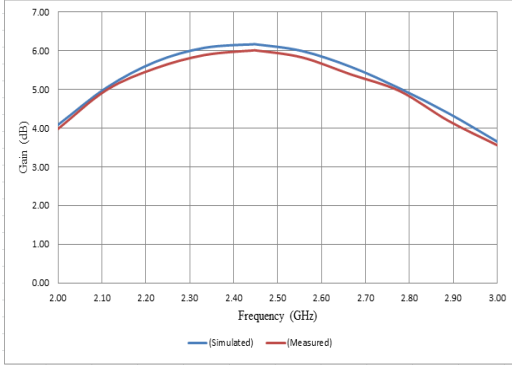


Figure 6. Simulated and measured Gain Vs Freq.

The calibrated two port Vector Network Analyzer (N9923A) is used to measure the S-parameters (S_{11} , S_{12} or S_{21} , S_{22}). The measured return loss for the feed point 1 is shown in Figure 7 and is below -15 dB over 169.2 MHz.

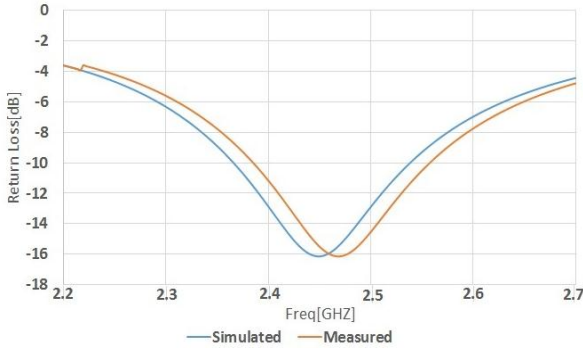


Figure 7. Simulated and measured return loss vs Freq. of prototype antenna

Table 6 displays the comparisons of simulated and measured results for the feed point 1 and 2. It is observed that, both the feed points were identical.

Table 6: Comparison of proposed antenna parameters

Parameters	Feed Point 1		Feed Point 2	
	Simulated	Measured	Simulated	Measured
Resonant Freq. (GHz)	2.45	2.53	2.45	2.53
Gain (dB)	6.17	6.01	6.17	6.01
S_{11} (dB)	-16.12	-15.34		
S_{22} (dB)			-16.11	-21.35
BW (MHz)	171.9	169.2	181.3	179.9
S_{12} or S_{21} (dB)	-19.60	-21.35	-19.60	-21.35
Phase (degrees)	90.71	87.92	90.71	87.92
VSWR	1.370	1.414	1.371	1.076

Table 7 demonstrates a comparison of various radiating elements for the Massive MIMO BS. It is seen from our design, by using coaxial probe-feed, CP, suspended substrate, slits loading on the patch and without using an antenna array the single pentagonal element exhibits a gain of 6.17 dB per port with impedance bandwidth of 171.9 MHz.

TABLE 7 : BENCHMARKING RESULTS OF THE ELEMENT WITH LITERATURE

Referenced elements	Operating Freq. (GHz)	BW (MHz)	Gain (dB)
[6]	3.6	230	5.4 / port (2 × 2 antenna array)
[10]	3.7	185	--
[11]	5.8	200	13 / port (1 × 4 antenna array)
[12]	2.596	194	10 / port (1 × 4 antenna array)
[16]	2.6	50	--
Proposed element	2.45	171.9	6.17 / port (without antenna array)

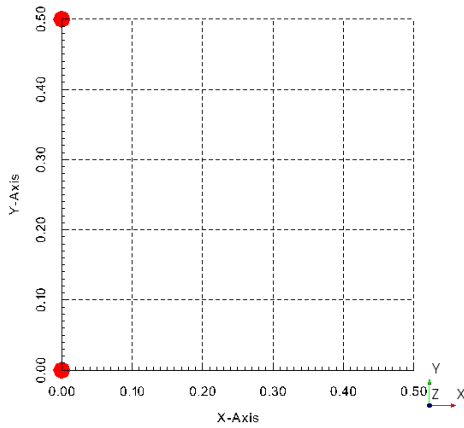
E. ANTENNA ARRAY GEOMETRY FOR MASSIVE MIMO BS

The basic objective of this section is to estimated the inter-lemnet spacing between the radiating elements. The inter-element spacing between the elements is very important while desinging the MIMO and Massive MIMO antennas for BS. It tells about the transmission/reception of independent signals in rich scattering. In such cases, the antenna array performance is done through spatial diversity. In this section, the linear (1D) and planar (2D) antenna array geometry where the radiating elements are placed along a line or along a both axis is considered for the Massive MIMO BS. The analysis of the linear antenna array is done using the systemVue software for isotropic elements in terms of maximum directivity (D_0), half-power beamwidth (HPBW), and side lobe level (SLL). The D_0 and HPBW (θ_h) of linear antenna array can be estimated by using equation (6) and (7) respectively [19].

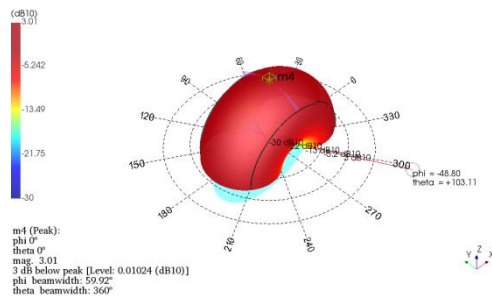
$$\theta_h \cong 2 \left[\frac{\pi}{2} \cos^{-1} \left(\frac{1.391\lambda}{\pi Nd} \right) \right] \quad (6)$$

$$D_0 \cong 2N \left(\frac{d}{\lambda} \right) \quad (7)$$

Where, N is the number of elements, d is the inter-element spacing, and λ is the operating wavelength. The linear antenna array geometry and its 3D radiation is shown in Figure 8. Two isotropic elements placed along y-axis. The total E-field radiated from the two elements at far-field will be $E_t = E_1 + E_2$.



(a) Antenna geometry



(b) 3D radiation pattern (Isometric view)

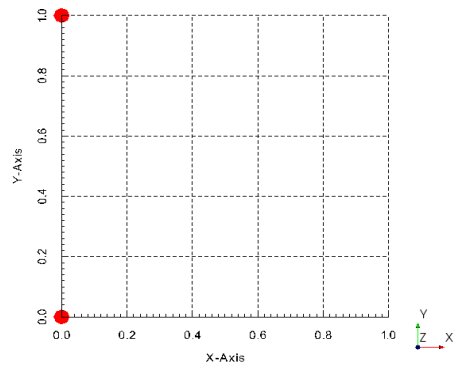
Figure 8. Linear antenna array ($N=2$, $d_y = 0.5\lambda$, $\beta_y = 0^\circ$)

The total patten obtained (Figure 8 b) for $N = 2$ is broadside (maxima is normal to the array axis or $\theta_0 = 90^\circ$). To achieve the broadside pattern, the phase of each element must be set to 0° (i.e., $\beta_y = 0^\circ$). Table 8 gives the comparison of simulated (using systemVue) and theoretical (using equ. (6) and (7)) results for linear antenn array ($N = 2$) with interelemnt spacing were vairred from 0.5 to 0.8.

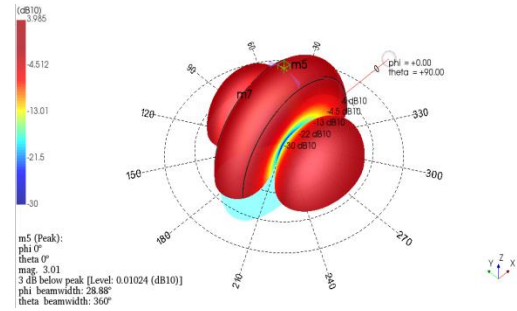
Table 8 Linear antenna array ($N = 2$, $\beta_y = 0^\circ$)

d_y	Directivity (dB)		θ_h (HPBW)		SLL (dB)
	Simulated	Theoretical	Theoretical	Simulated	
0.5	3.01	3.01	59.92	52.59	-
0.6	3.74	3.80	49.16	43.32	-
0.7	4.06	4.47	41.8	36.89	0.547
0.8	3.92	5.05	36.35	32.14	2.08

Figure 9 and 10 shows the effect of inter-element spacing for $N = 2$ elements.

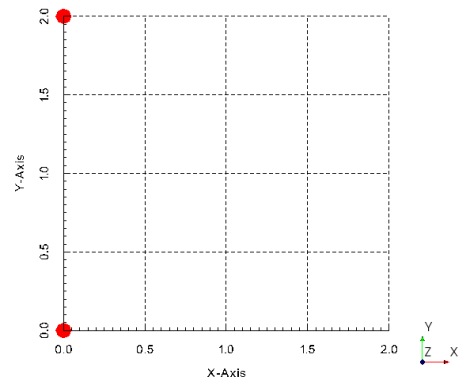


(a) Antenna geometry

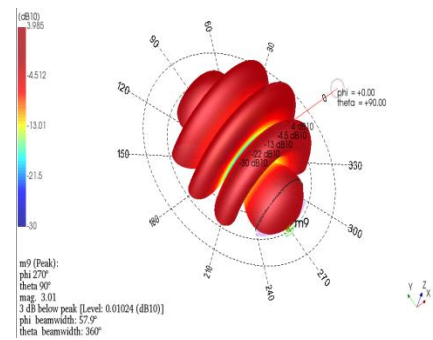


3D radiation pattern (Isometric view)

Figure 9. Linear antenna array ($N=2$, $d_y = 1\lambda$, $\beta_y = 0^\circ$)



(a) Antenna geometry



(b) 3D radiation pattern (Isometric view)

Figure 10. Linear antenna array ($N=2$, $d_y = 2\lambda$, $\beta_y = 0^\circ$)

It is observed from Table 8 that, as the inter-element spacing between the elements increased, the D_0 increases, but HPBW decreases (since $D_0 \propto \frac{1}{HPBW}$). We also observed that the SLL slowly increases for spacing beyond $d_y = 0.6\lambda$. From Figure 9 and 10, we observed that as the inter-element spacing increased beyond 1λ , an antenna array produces grating lobes (multiple maxima) with increased SLL. Simulation results for inter-element spacing ($d_y < \frac{\lambda}{2}$) were also checked and gives the grating lobes. Thus, in order to avoid aliasing, any grating lobes and causing of nulls to be misplace, the inter-element spacing should satisfy the condition ($\frac{\lambda}{2} < d_y < \lambda$).

Similarly, we have observed for $N = 4$ and 8 elements with $\beta_y = 0^\circ$ and their simulated results are tabulated in Table 9 and 10.

Table 9: Linear antenna array ($N = 4$, $\beta_y = 0^\circ$)

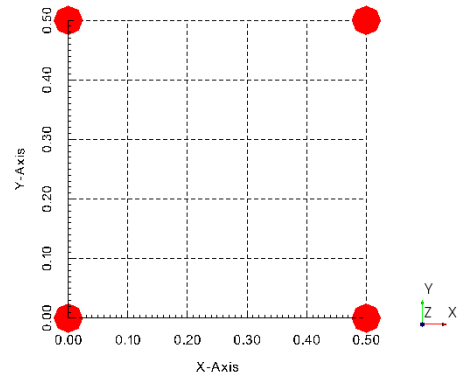
d_y	Directivity(dB)		θ_n (HPBW)		SLL (dB)
	Theoretical	Simulated	Theoretical	Simulated	
0.5	6.02	6.02	25.59	26.28	-5.28
0.6	6.81	6.72	21.27	21.85	-4.57
0.7	7.48	7.18	18.19	18.66	-4.11
0.8	8.06	7.71	15.9	16.31	-3.59

Table 10: Linear antenna array ($N = 8$, $\beta_y = 0^\circ$)

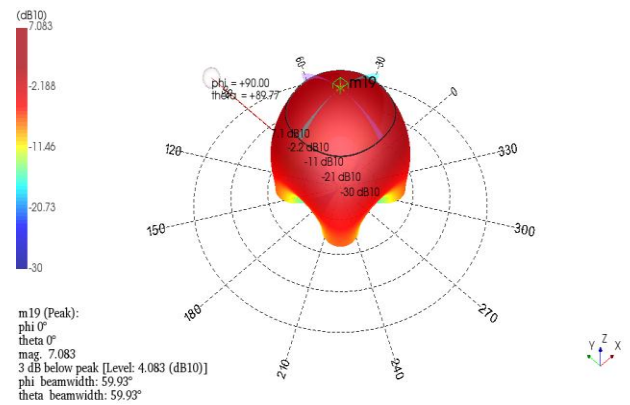
d_y	Directivity(dB)		θ_n (HPBW)		SLL (dB)
	Theoretical	Simulated	Theoretical	Simulated	
0.5	9.03	9.03	12.71	12.72	-3.76
0.6	9.82	9.75	10.58	10.58	-3.04
0.7	10.49	10.36	9.06	9.03	-2.44
0.8	11.07	10.85	7.93	7.97	-1.94

It is observed from Table 9 and 10 that, as the number of elements increased, the D_0 also increases. Through the simulations, we observed that, the inter-element spacing between the radiating elements can be chosen as 0.5 or 0.6 for the Massive MIMO BS. More number of radiating elements can not be placed if the inter-element spacing is greater than 0.7. Inter-element spacing > 0.7 helps to increase the isolation among the radiating elements.

Figure 11 shows the 2×2 planar antenna array geometry (in systemVue) and its total radiation pattern. It gives, $D_0 = 7.03$, HPBW = 59.93° , and no SLL.



(a) Antenna geometry (2×2 , $dx = dy = 0.5$, $\beta_x = \beta_y = 0^\circ$)



(a) 3D radiation pattern (Isometric view)

Figure 11. Planar antenna array

The planar antenna array geometry (in HFSS) is shown in Figure 12. It consists of 4 RHCP radiating elements. The inter-element spacing was kept as 0.5 (estimated using systemVue).

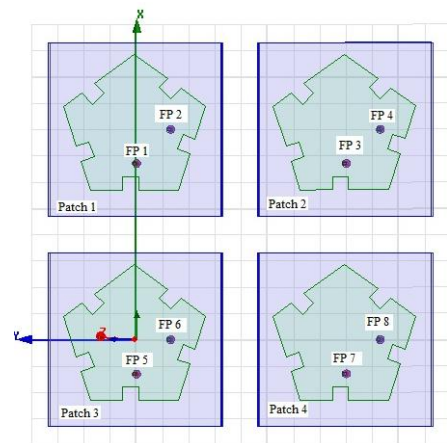


Figure 12. Planar antenna array (2×2 , $dx = dy = 0.5$)

The simulated return loss (S_{11} to S_{88}) and mutual coupling or isolation (S_{11} , S_{31} , S_{51} , S_{71}) for the 2×2 planar array using HFSS are shown in Figure 13 and 14 respectively. Each port

shows better return loss (< -18 dB). The isolation among the ports (S_{11} , S_{31} , S_{51} , S_{71}) are greater than 20 dB. Isolation > 20 dB is also observed for other ports (S_{22} , S_{24} , S_{26} , S_{28}).

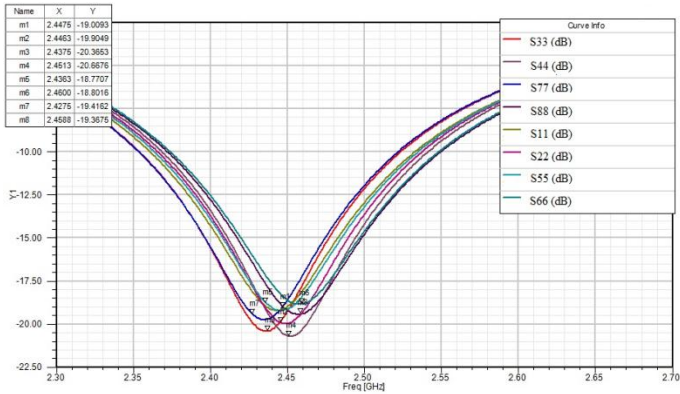


Figure 13. Simulated S –parameters (S_{11} to S_{88})

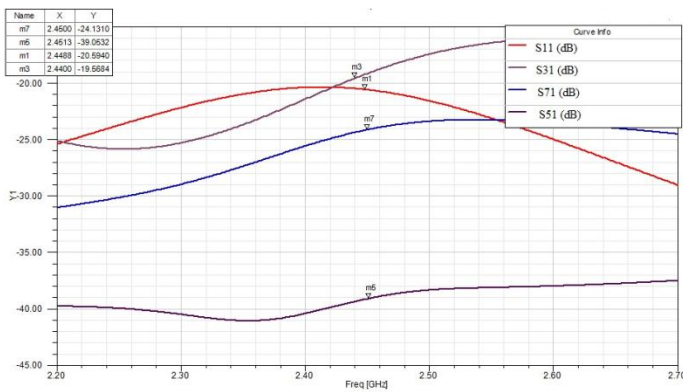


Figure 14. Simulated S –parameters (S_{11} , S_{31} , S_{51} , S_{71})

F. CONCLUSIONS

A printed pentagonal microstrip antenna is suitable for Massive MIMO BS antenna was presented. The five slits were optimized and using the suspended substrate, the antenna’s gain (6.17 dB) and impedance bandwidth (171.9 MHz) is enhanced. The AR 1.78 (< 3 dB) with bandwidth of 135 MHz was achieved. The HFSS and experimental results are found to be in good agreement. The inter-element spacing of linear and planar antenna array for the Massive MIMO BS were optimized using systemVue. The 2×2 MIMO antenna exhibits return loss (< -18 dB) and greater isolation (> 20 dB).

G. Future Work

The Massive MIMO BS antenna will be developed by mounting 64 pentagonal microstrip elements (or 128 ports). Using the spatial and polarization diversity, correlation among the radiating elements can be minimized. These

elements will be placed on each side of the octagonal shaped architecture. Each side consists of 8 elements (2×4 antenna array). The reason behind the octagonal shaped architecture for Massive MIMO BS is that, it uses space more efficiently. Also, this structure will be suitable for Smart antennas.

REFERENCES

1. Hong-Wei Yuan, Guan-Feng Cui, and Jing Fan —“A Method for Analyzing Broadcast Beamforming of Massive MIMO Antenna Array” Progress In Electromagnetics Research Letters, Vol. 65, 15–21, 2017.
2. Paul Harris, Student Member, IEEE, Steffen Malkowsky, Student Member, IEEE, Joao Vieira, Erik Bengtsson, Fredrik Tufvesson, Fellow, IEEE, Wael Boukley Hasan, Student Member, IEEE, Liang Liu, Member, IEEE, Mark Beach, Member, IEEE, Simon Armour, and Ove Edfors, Member, IEEE —“Performance Characterization of a Real-Time Massive MIMO System With LOS Mobile Channels” IEEE Journal on selected areas in Communications, Vol. 35, No. 6, June 2017.
3. Xiaohu Ge, Senior Member, IEEE, Ran Zi, Student Member, IEEE, Haichao Wang, Jing Zhang, Member, IEEE, and Minh Jo, Member, IEEE —“Multi-User Massive MIMO Communication Systems Based on Irregular Antenna Arrays” IEEE Transactions on Wireless Communications, Vol. 15, No. 8, August 2016.
4. Akshay Jain and Sandeep K. Yadav —“Design and Analysis of Compact 108 Element Multimode Antenna Array for Massive MIMO Base Station” Progress In Electromagnetics Research C, Vol. 61, 179–184, 2016.
5. Pierluigi Vito Amadori, Student Member, IEEE, and Christos Masouros, Senior Member, IEEE —“Interference-Driven Antenna Selection for Massive Multiuser MIMO” IEEE Transactions on Vehicular Technology, Vol. 65, No. 8, August 2016.
6. Monjed A. Al-Tarifi, Yanal S. Faouri, and Mohammad S. Sharawi, —“A Printed 16 Ports Massive MIMO Antenna System with Directive Port Beams”, IEEE 5th Asia-Pacific Conference on Antennas and Propagation (APCAP), pp.125-126, 2016.
7. E. G. Larsson, O. Edfors, F. Tufvesson, and T. L. Marzetta, —“Massive MIMO for Next Generation Wireless Systems,” IEEE Communications Magazine, vol. 52, no. 2, pp. 186–195, 2014.

8. F. Boccardi, R. W. Heath, A. Lozano, T. L. Marzetta, and P. Popovski, "Five Disruptive Technology Directions for 5G," *IEEE Commun. Mag.*, vol. 52, no. 2, pp. 74–80, Feb. 2014.
9. Yulin Zheng, Guang Hua, Houxing Zhou, Wei Hong, —"Research of Multi-beams Antenna Array Using Butler Matrix in MIMO Communication" 3rd Asia-Pacific Conference on Antennas and Propagation, IEEE, 978-1-4799-4354-8/14/\$31.00, 2014.
10. Vieira, J., Malkowsky, S., Nieman, K., Miers, Z., Kundargi, N., Liu, L., ... Tufvesson, F. —"Aflexible 100- antenna testbed for Massive MIMO".IEEE Globecom Workshop, 2014, Austin, Texas, United States.
11. PANG Xingdong, HONG Wei, YANG Tianyang, LI Linsheng —"Design and Implementation of an Active Multibeam Antenna System with 64 RF Channels and 256 Antenna Elements for Massive MIMO Application in 5G Wireless Communications" *China Communications*, pp. 16-22, November 2014.
12. Younsin Kim, Hyoungju Ji, Juho Lee, Young-Han Nam, Boon Loong Ng, Ioannis Tzanids, Yang Li, and Jianzhong (Charlie) Zhang "Full dimension MIMO (FD-MIMO): the next evolution of MIMO in LTE systems", *IEEE Wireless Communications*, pp. 26-33, April 2014.
13. H. Q. Ngo, E. Larsson, and T. Marzetta, —"Energy and spectral efficiency of very large multiuser MIMO systems" *IEEE Transactions on Communications* , vol. 61, no. 4, pp. 1436–1449, April 2013.
14. Jakob Hoydis, Stephan ten Brink, and Marouane Debbah, —"Massive MIMO in the UL/DL of Cellular Networks: How Many Antennas Do We Need?," *IEEE Journal on Selected Areas in Communications*, vol. 31, no. 2, pp.160-171, February 2013.
15. Telecom Regulatory Authority of India (TRAI), New Delhi 30th October, 2012.
16. S. Payami and F. Tufvesson, —"Channel measurements and analysis for very large array systems at 2.6 GHz," in *European Conf. Antennas and Propagation (EUCAP' 2012)*, Prague, pp. 433–437, Mar. 2012.
17. Veeresh G. Kasabegoudar and K. J. Vinay, —"Cplanar Capacitively Coupled Probe Fed Microstrip Antennas for Wideband Applications", *IEEE Transactions on Antennas and Propagation*, Vol. 58, No. 10, pp.3131-3138, October 2010.
18. V. G. Kasabegoudar and K. J. Vinay, —"A Broadband Suspended Microstrip Antenna for Circulation Polarization", *Progress in Electromagnetics Research, PIER 90*, pp. 353–368, 2009.
19. Balanis, C. A., *Antenna Theory*, John Wiley & Sons, Inc., New York, 2004.
20. Garg, R., P. Bhartia, I. Bahl, and A. Ittipiboon, *Microstrip Antenna Design Handbook*, Artech House, Norwood, MA, 2001.